On-Axis Bunch Extraction from an Antiproton Plasma Reservoir

CERN Summer Student Programme
IPP Summer Student Fellowship

Meghan Naar[1]
August 24, 2025

Supervised by: Dr. Eric Hunter[2], Dr. Chloé Malbrunot[1]

[1]TRIUMF, Vancouver, Canada
[2]CERN, Geneva, Switzerland

1 Introduction

The Standard Model of particle physics is a description of known particles and their interactions. It also summarizes fundamental symmetries in the universe like CPT symmetry, which is the combined operation of charge conjugation (C), parity transformation (P), and time reversal (T). The CPT theorem [1] establishes that any local, Lorentz-invariant quantum field theory must conserve CPT symmetry, implying that particles and their antiparticles must have equal or opposite fundamental properties like charge. However this prediction is at odds with the observed imbalance of matter and antimatter in the universe. According to Sakharov [2], such an imbalance requires three conditions including CP violation - but the amount of CP violation observed so far is too small to account for the matter-antimatter asymmetry. This motivates increasingly precise tests of CPT symmetry. Many experiments are doing so at CERN's Antimatter Factory - comprised of the AD (Antiproton Decelerator) and ELENA (Extra Low Energy Antiproton ring) - to experimentally compare matter and antimatter properties.

ASACUSA (Atomic Spectroscopy And Collisions Using Slow Antiprotons) is a joint collaboration of two experiments which both aim to test CPT symmetry. ASACUSA-1 uses laser spectroscopy on antiprotonic helium atoms to measure the antiproton-to-electron mass ratio [3], and ASACUSA-2 measures the ground-state hyperfine structure of antihydrogen ($\bar{\mathrm{H}}$) [4]. ASACUSA-2 uses three-body recombination ($\mathrm{e}^+ + \mathrm{e}^+ + \bar{\mathrm{p}} \rightarrow \bar{\mathrm{H}} + \mathrm{e}^+$) of positrons ($\mathrm{e}^+$) and antiprotons ($\bar{\mathrm{p}}$) to create $\bar{\mathrm{H}}$ that pass through a spectroscopy apparatus for hyperfine structure measurements, as shown in Fig. 1. Since three-body recombination creates highly excited states of $\bar{\mathrm{H}}$, they must have time to deexcite to the ground state on their way to the spectroscopy apparatus to maximize the signal to noise ratio. This requirement imposes constraints on the velocity of the $\bar{\mathrm{H}}$ atoms.

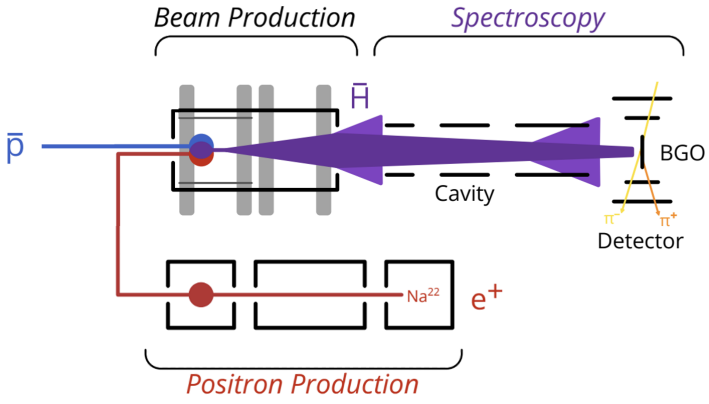

Figure 1: *Schematic diagram of the ASACUSA-2 experiment [5]. $\bar{H}$ are formed in the trap - by combining $\bar{p}$ from ELENA and e^+ from a ^{22}Na source - and some of them go through the spectroscopy apparatus consisting of a microwave cavity and detector containing a BGO crystal.*

By catching and trapping low-energy antiprotons from ELENA, each experiment can form atoms that cannot be created at any other facility worldwide. This report discusses a novel $\bar{\mathrm{H}}$ production technique being investigated by ASACUSA-2.

2 Antihydrogen Production

2.1 Slow Merge

ASACUSA has shown success in making $\bar{H}$ using a so-called "slow merge" technique pioneered by the ATRAP and ALPHA collaborations [6], [7]. In this technique, both e^+ and $\bar{p}$ are confined using electric and magnetic fields in Penning-Malmberg [8] traps. A magnetic field confines the particles radially, while an electric field traps the particles axially; electrostatic potential wells are created by a set of individually biasable coaxial cylinders, or electrodes. Slow e^+ from a ^{22}Na source as seen in Fig. 1 are caught in a negative potential well, and $\bar{p}$ get trapped in positive wells once they arrive from ELENA. During mixing, e^+ and $\bar{p}$ are in adjacent wells and slowly brought into contact by reducing the depths of the electrostatic potentials until both particle types sit at the same potential. Figure 2 shows the electrostatic potentials for a standard mixing cycle in this method, including the corresponding biasable electrodes.

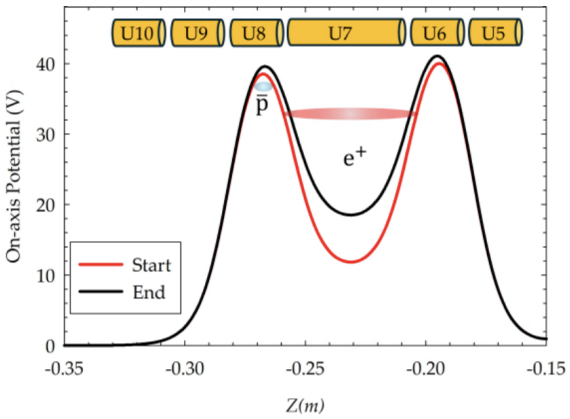

Figure 2: *Axial electric potentials used to confine the e^+ and $\bar{p}$ plasmas before (red line) and after (black line) mixing in the slow merge scheme [5]. During the slow merge, both particle types sit at the same potential. The electrodes used to create such potentials are shown above in yellow, though only U7 is changed between the red and black curves.*

This is a known, reliable way to make $\bar{H}$ since the collaboration had success with this method in the past: at the end of beam time in 2024, on the order of 10,000 $\bar{H}$ atom candidates were detected in a 24 hour period upon using the slow merge method [5]. However, in this scheme $\bar{H}$ is produced isotropically, with over 99% of atoms annihilating in the trap rather than forming a usable beam for spectroscopy measurements [9].

2.2 The Beam Scheme

The beam scheme is a new proposed method for $\bar{H}$ production. Unlike a slow merge process where the e^+ and $\bar{p}$ are brought into contact at a given potential, the beam scheme aims to shoot a small bunch or "scoop" of $\bar{p}$ along the z-direction - aligned with the magnetic field - through the e^+ plasma, as illustrated in Fig. 3.

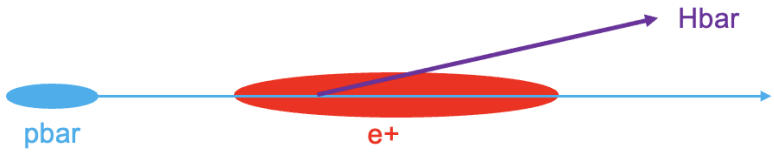

Figure 3: *Graphical depiction of the beam scheme where a small plasma of $\bar{p}$ (blue) is sent through the e^+ well (red), creating outgoing $\bar{H}$ (purple).*

Here, the e^+ plasma containing $\mathcal{O}(10^8)$ e^+ sits in a potential well downstream of the $\bar{p}$ reservoir (not shown in Fig. 3) holding $\mathcal{O}(10^7)$ $\bar{p}$ and $\mathcal{O}(10^8)$ electrons. Scoops are formed by changing the voltage on the electrodes to break off a portion of the $\bar{p}$ reservoir. These scoops are then sequentially sent down the trap through the e^+ until the $\bar{p}$ reservoir is depleted. This technique may give a higher yield of detectable $\bar{H}$ since most of the atoms are already moving in the right direction towards the spectroscopy apparatus. Additionally, this technique is attractive because one knows precisely when $\bar{p}$ pass through the e^+ reservoir, which gives insight on when $\bar{H}$ are formed: directly after the e^+ well, the magnetic field diverges causing $\bar{p}$ to move radially outward and annihilate on the walls of the trap. This process happens quickly, meaning $\bar{H}$ formation is $\mathcal{O}(10^{-6})$s before the $\bar{p}$ annihilation signal. Since $\bar{H}$ atoms travel 2.5 m to the detector at an energy of 5 meV, corresponding to a drift time on the order of 10^{-3}s, this uncertainty is negligible.

Using this information, one can calculate the speed of each $\bar{H}$ atom. Knowing the formation time of $\bar{H}$ from $\bar{p}$ annihilations, the time $\bar{H}$ hit the BGO crystal detector, and the distance between the two, an average velocity can be found. Selecting low-velocity atoms will improve the signal-to-noise ratio in spectroscopy measurements. The beam scheme will homogenize the velocity of the formed $\bar{H}$, allowing for optimal conversion from excited hyperfine states to ground state in the cavity [10].

While the beam scheme offers significant experimental advantages, it is technically challenging. As in the slow merge method, maximizing $\bar{H}$ yield requires the e^+ plasma to be both dense and extremely cold - on the order of tens of kelvin [11]. The incoming $\bar{p}$ must also be precisely controlled: they must be aligned within 0.1 mm of the trap axis to pass through the densest region of the e^+ plasma, and finely tuned energy in the z-direction to maximize interaction time with the cold e^+ [11]. The present work focuses on ensuring the scoops are extracted from the reservoir on-axis.

3 The Magnetron Problem

The signature of off-axis scoops is their magnetron motion. When charged particles are under the influence of a magnetic field, they undergo two distinct radial motions: cyclotron and magnetron orbits. Cyclotron orbits are smaller, rapid motions due to the Lorentz force with a frequency given by,

$$\omega_c = \frac{qB}{m} \tag{1}$$

where q is the charge, B is the magnetic field strength, and m is the mass. Magnetron orbits however, are due to the combined presence of electric and magnetic fields. Under the influence of both electric and magnetic fields, the particles experience an $\mathbf{E} \times \mathbf{B}$ drift, perpendicular to both fields. In the trap, the magnetic field is aligned along the axis, with a radially inward electric field that causes scoops to orbit the central axis. The magnetron frequency is given by,

$$\omega_m = \frac{\omega_c \pm \sqrt{\omega_c^2 - 2\omega_z^3}}{2} \approx \frac{\omega_z^2}{2\omega_c} \tag{2}$$

where $\omega_z = \sqrt{2ek_2/m}$ is the harmonic motion of the plasma in z where $k_2 = \frac{\partial^2 U}{\partial z^2}$ is the trap depth constant and U is the electric potential inside the trap. The approximation on ω_m is valid in the limit $\omega_z \ll \omega_c$, which is the case in this trap. This motion can be large compared to the plasma radius, and the goal is to ensure that scoops are extracted from the reservoir with minimized magnetron motion for transfer to the center of the e^+ plasma.

Because this issue has not yet been studied in detail by the collaboration, there is no established method for reduction of magnetron orbital radius. Potential approaches include adjusting the plasma compression parameters, modifying the timing of the preparation and scooping steps, or changing the electrostatic potentials used to extract the scoops.

The timescale for preparing a $\bar{p}$ plasma is too long for rapid testing: it takes roughly 15 minutes to collect $\bar{p}$ from ELENA, transfer them to the mixing trap, and extract scoops from the reservoir. Electrons (e^-) provide a practical alternative for $\bar{p}$ due to their identical charge. With a local e^- source in ASACUSA, a single run can be completed in only a few minutes. This study uses e^- for development, with the results later applied to $\bar{p}$.

4 Methodology

4.1 Plasma Manipulation

Scoops of e^- are produced by breaking off a portion of the reservoir using electrostatic potential manipulations. The original scooping mechanism, developed prior to this work and shown in Fig. 4, follows the technique described in [12].

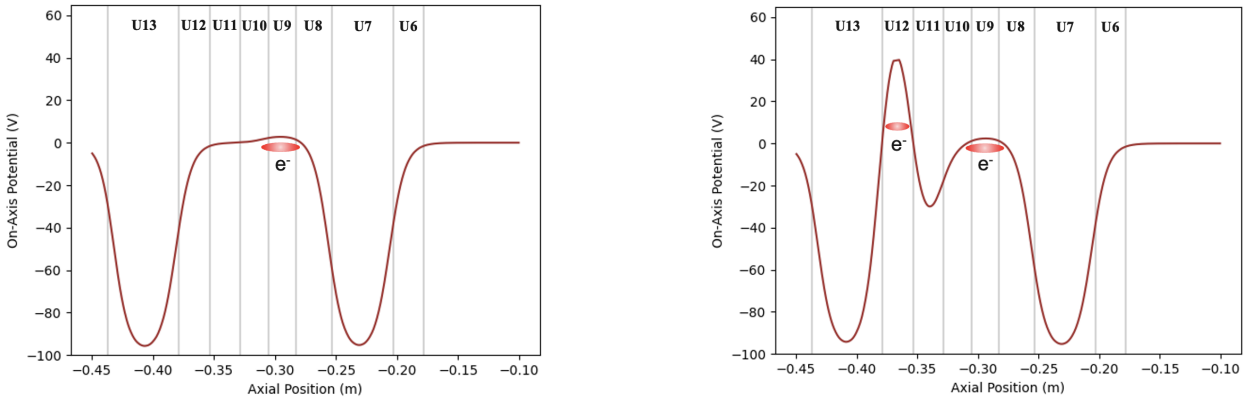

Figure 4: *Electric potentials before (left) and after (right) scooping, including the electrodes used to create the potentials as well as the location of e^-.*

These potentials are designed to hold both e^- (or $\bar{p}$) and e^+ simultaneously. Though e^+ are not used in this work, they would sit in the negative potential of electrode U7. e^-, however, are initially confined in electrodes U8 & U9. Scooping is a simultaneous decrease in potential on U11 and increase on U12, both breaking the scoop off the reservoir and isolating it in a deep well. Here, the depth of the U12 well is taken to be arbitrarily large, a choice that has proven effective in previous studies. The scooping mechanism shown in Fig. 4 originally took 100 ms.

As e^- are scooped out of the reservoir, the level of the reservoir (or how full it is) will decrease. To counteract that, the bottom of the reservoir is shifted to a slightly lower potential after every scoop. This ensures that there will always be e^- at such a level which will be cut off by the scooping potential.

In this work, a new scooping method was investigated by splitting the potentials in Fig. 4 into three distinct steps shown in Fig. 5.

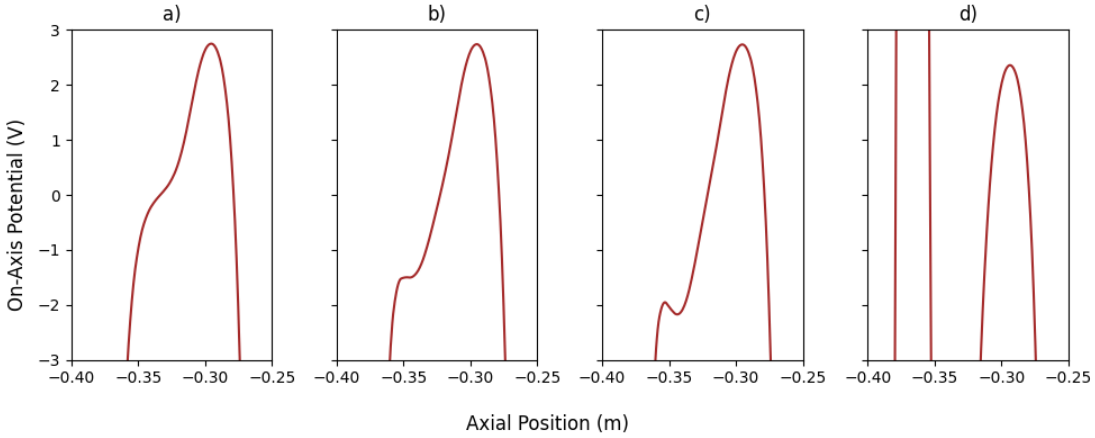

Figure 5: *Graphical depiction of the electrostatic potentials a) before scooping, b) after pre-scoop, c) after scooping, and d) after well deepening steps.*

The initial potential (a) is followed by the pre-scoop (b), scoop (c), and well deepening (d) motions. First, step b) creates a level barrier in U11. Here, no e^- are broken off of the well, they are simply brought to a lower potential. Next, step c) breaks off a piece of the reservoir by reducing the potential in U11, creating a shallow well in U12 to hold e^-. Lastly, the well in U12 is made very deep in step d) to isolate the scoop.

The magnetron frequency of particles confined in each potential well in Fig. 5 can be estimated using the approximation in Eq. 2. Trap frequencies are summarized in Table 1 (units: Hz) for e^-: since particle mass cancels in the calculation of ω_m, the magnetron frequency for e^- and $\bar{p}$ is the same. The reciprocal of the magnetron frequency in the scoop well (1 ms) will be an important timescale in this work.

	Reservoir	Scoop Well	Deeper Well
$\omega_z/2\pi$	5×10^6	8×10^6	36×10^6
$\omega_c/2\pi$	4.2×10^{10}	2.8×10^{10}	2.4×10^{10}
$\omega_m/2\pi$	2.3×10^2	1.1×10^3	2.7×10^4

Table 1: *Summary of trap frequencies (in Hz) for e^- in various potential wells in Fig. 5.*

4.2 Detection & Analysis

Though the beam scheme sends $\bar{p}$ downstream towards U7, these tests send e^- upstream to a microchannel plate (MCP) detector. The charge cascade created by e^- striking the MCP then hits a phosphor screen directly behind the MCP. A CMOS camera finally captures an image of the light from the phosphor screen which is used for analysis. In this work, one image is taken per scoop.

To quantify the magnetron motion, the average position of the e^- or $\bar{p}$ inside the scoop when extracted towards the MCP was measured using a center-finding algorithm. This will be referred to as the "scoop center" which has coordinates (x_i, y_i) for each scoop. From the scoop centers, the mean scoop position was calculated with coordinates (x_{mean}, y_{mean}). Finally, the distance from each scoop center to the average scoop position, d_i, was calculated as follows.

$$d_i = \sqrt{(x_{mean} - x_i)^2 + (y_{mean} - y_i)^2} \tag{3}$$

The center-finding algorithm employed a center-of-mass approach to find the brightest spot in the image, allowing for sub-pixel resolution. This is not as straightforward as it may seem. Ideally, the weighted sum gives the exact center of the plasma, but the camera produces "hot pixels" which are single bright pixels among the dark background, skewing the calculated center. Three steps are employed in this work to remove hot pixels. First, the camera bins pixels by 4. Then, for each pixel, a local mean is computed over a 5×5 size neighbourhood. Any pixel exceeding two times of this local mean is flagged as a hot pixel. Flagged pixels are replaced with the corresponding local mean, producing a "cleaned" image. Lastly, a final step identifies the main bright region of the image: the background is estimated as the median pixel value of the cleaned image, and a threshold is set slightly above this background. Pixels above this threshold are defined as the plasma, ensuring only the correct region of the image contributes to the center calculation.

5 Results

5.1 Electrons

A total of 100 scoops were taken from the reservoir to ensure enough data for analysis. Fig. 6 shows an example plasma taken at the beginning and end of data collection, along with their calculated centers.

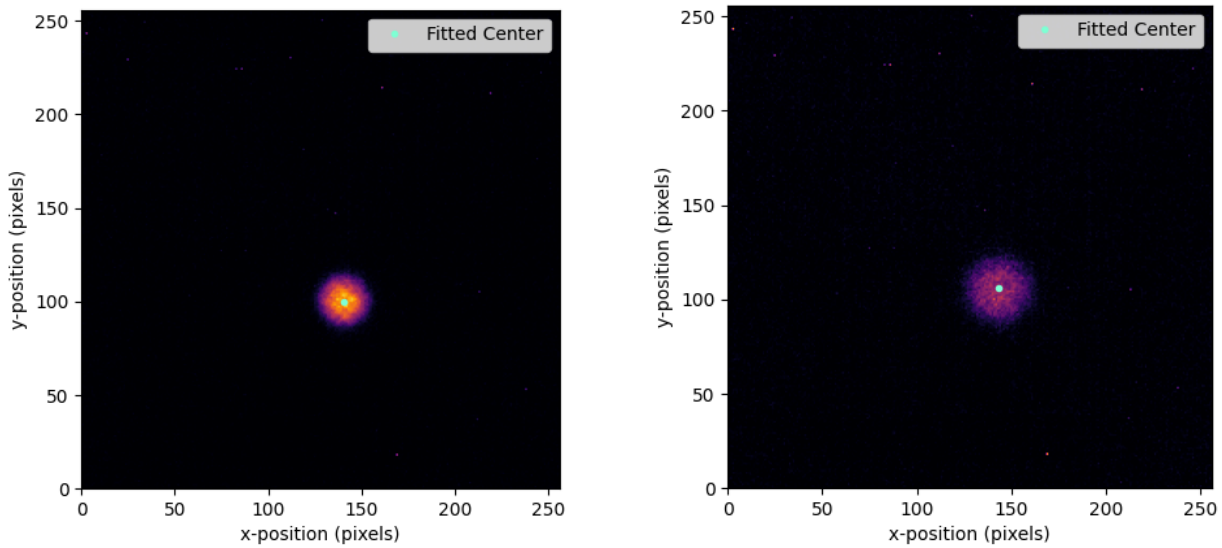

Figure 6: *Sample initial and final e^- plasma images collected by the CMOS camera during 100 scoops, showing how plasma radius increases with every scoop. Fitted centers for each plasma are shown in green.*

In an effort to reduce magnetron orbital radius, the timing of plasma manipulations in Fig. 5 was optimized. It was found that step c) (scooping) must be performed slowly to reduce magnetron, though steps b) and d) could be as fast as 10 ms. Scooping was initially lengthened to 200 ms, which showed a clear decrease in magnetron motion. As mentioned above, the period of the magnetron motion is on the order of 1 ms, meaning that perturbations of the same order may cause the size of the orbit to change. Slower perturbations preserve the adiabatic invariant associated with this motion and therefore should not cause magnetron orbital radius to change [13].

With an established mechanism for reducing magnetron motion, the next step is optimization - specifically, identifying the shortest scoop time that still produces centralized scoops. Faster scoops are preferable, as this will allow the entire $\bar{p}$ well to be emptied in a reasonable timescale. Scoop times were tested in 10 ms increments from 120 ms to 10 ms, as shown in Fig. 7, showing that scooping for 70 ms or longer is optimal for minimizing magnetron motion.

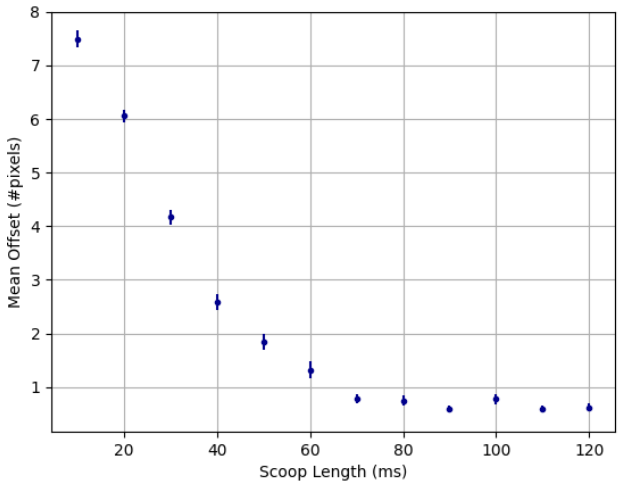

Figure 7: *Scan of the mean offset of scoops from their mean value as a function of scoop time.*

Beyond adjusting scoop time, other parameters of the process were optimized. Previously, the reservoir was compressed after every scoop to maintain small scoop sizes. This however, significantly increased the run time. The compression step is now performed after every 100 scoops, which was found to be the optimal value to ensure reasonably-sized final plasmas before recompression. The scooping well depth as seen in Fig. 5c) was also reduced from 2.1 V to 0.16 V while maintaining reasonable scoops.

Figure 8 shows the distribution of scoop centers and the average scoop position for both fast- and slow-scooping datasets using the optimized method. The positions are overlaid on the space of a sample CMOS camera image, with separations measured in pixels, where 1 pixel $\approx$ 0.33 mm.

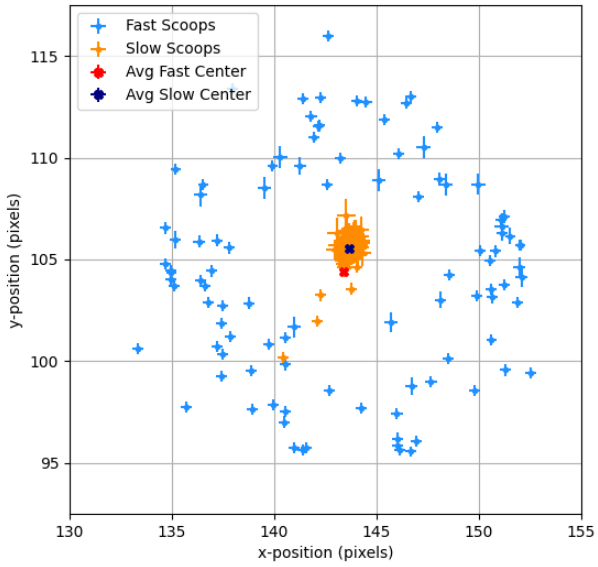

Figure 8: *Plot of 100 scoop centers for both a fast (blue) and slow (orange) scooping dataset as collected by the CMOS camera. The average scoop position for the fast dataset is shown in red, and in navy blue for the slow dataset.*

Fig. 8 shows a clear improvement between scooping quickly versus slowly. Fast scooping results in a clear ring of scoop positions. These data have an average distance to the mean scoop position, or "offset" of 7.49 ± 0.15 pixels or $\approx 0.25 \pm 0.005$ mm from center. Scooping slowly however, significantly decreases offsets to 0.61 ± 0.07 pixels or $\approx 0.02 \pm 0.002$ mm. This is an exciting result, showing it's possible to reduce e^- magnetron motion to below 0.1 mm.

This result is yet to be understood however, as there is no clear mechanism which would explain this phenomenon. The effect may be related to a two-stream instability [14], where co- and counter-streaming particles interact and form a "bubble" in phase space that extracts energy and traps particles. It could be that if the scoop is done too quickly, the phase space bubble forms and evolves while the scoop is being isolated, potentially breaking the magnetron adiabatic invariant. Scooping slowly however, would allow the instability to saturate before the scoop well is separated from the reservoir.

5.2 Antiprotons

Once the optimal procedure was established for e^-, it was applied to $\bar{p}$ to evaluate its performance for the beam scheme. Initial tests used the same parameters as the e^- queue, but with three sets of 100 scoops, separated by 30 s compression and 10 s cooling steps. Example plasmas are shown in Fig. 9.

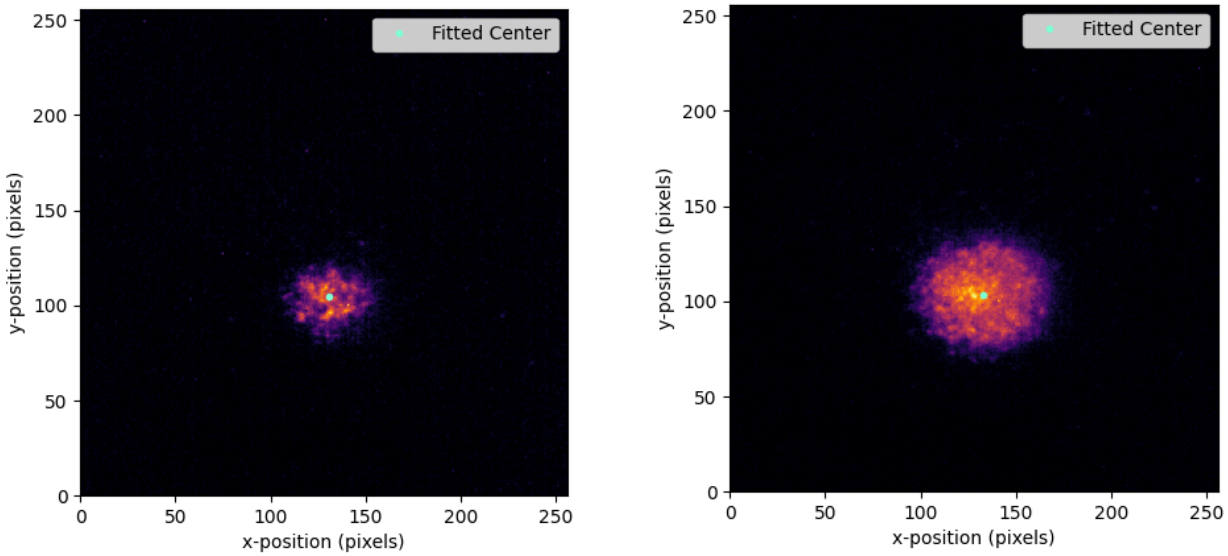

Figure 9: *Sample $\bar{p}$ plasma images from the beginning and end of data collection, along with their fitted centers in green.*

It is easy to see from these images that $\bar{p}$ plasmas are much larger than e^- plasmas, and face greater expansion throughout the scooping process. Expanded plasma profiles are dimmer and can be difficult to fit.

The scoop centers of the 300 $\bar{p}$ scoops were calculated to examine their magnetron orbit radius, with their distribution shown in Fig. 10.

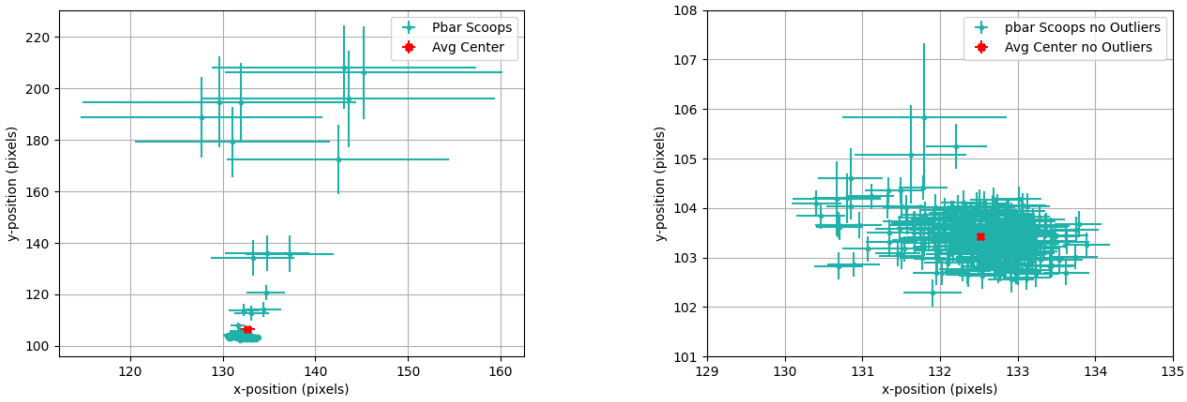

Figure 10: *Plots of scoop positions on the camera at the MCP for $\bar{p}$ (left), and positions without outliers (right).*

The center-finding algorithm struggles to find accurate centers for extremely dim plasmas, resulting in outlier positions as seen in the left plot in Fig. 10. By removing outlier scoops (right plot in Fig. 10), one can see a dense cluster of $\bar{p}$. Including outliers, the average offset of these scoops is 5.62 ± 0.81 pixels ($\approx 0.19 \pm 0.03$ mm), and excluding outliers gives an offset of 0.64 ± 0.03 pixels or $\approx 0.02 \pm 0.0009$ mm which is within the threshold required for the beam scheme. This confirms that the technique developed with e^- is also effective for $\bar{p}$.

Large $\bar{p}$ magnetron orbits observed during 2024 data collection have been reproduced in summer 2025, and reduced after implementing the technique in this work. Though these data confirm that the magnetron orbital radius can be reduced for $\bar{p}$, further work is needed to find their optimal scooping time.

6 Future Steps

Though this technique represents a major step forward for the beam scheme, there are still several technical challenges to overcome before $\bar{H}$ formation. While slow-scooping enables $\bar{p}$ to exit U12 almost perfectly on-axis, they may not enter the e^+ plasma in U7 at the same radial position. As magnetized particles travel through the trap, they follow magnetic field lines, and there is a possibility that the magnetic field lines exiting the center of U12 do not enter the center of U7. A proposed solution is to exploit the magnetron orbit and phase of the scoops. By deliberately displacing the $\bar{p}$ plasma off-axis in a controlled way by weakening the trapping potential [13], the scoops can be placed at the correct radial distance to pass through the center of the e^+ plasma. Any angular offset could then be corrected by timing their arrival so that they enter the e^+ well at the correct phase of their orbit. This technique may ultimately be unnecessary if the electrode centers are well aligned with the magnetic field, but it is a potential challenge.

Since the e^+ plasma is confined between trapping potentials, the $\bar{p}$ must still have enough energy to clear these barriers, ideally just "skimming" over the top. While this might seem straightforward, it's made difficult by the fact that $\bar{H}$ formation removes e^+ from the well, lowering its level after each pass. The optimal skimming potential then changes after every

scoop. Achieving this will require real-time feedback on the e^+ well's space charge and automatic adjustment of the trapping potentials - fast enough to keep up with the scooping process. A system to accomplish this is currently under development by the collaboration.

Finally, although this technique greatly reduces magnetron motion, further optimization is needed to produce cool, dense $\bar{p}$ scoops. The current scoops have a 0.4 mm radius and are $\approx$300 K in z (transverse temperature is not measured). Ref. [11] assumes a monoenergetic beam (T=0 K in the axial direction), and shows $\bar{p}$ must enter the e^+ plasma at r <0.1 mm. The long-term goal is to scoop the entire $\bar{p}$ reservoir for $\bar{H}$ production. For that, the limiting factor is the time required for compression steps, which must be kept within a reasonable timescale such that scooping out the entire reservoir takes approximately 20 minutes.

7 Conclusion

This work demonstrates a successful technique, applied to both e^- and $\bar{p}$ bunches, for reducing magnetron motion in preparation for a new scheme to produce a pulsed $\bar{H}$ beam. By increasing the time for the electric potentials to create a scoop, the average offset from center was reduced by a factor of 12 for e^-, though further work is needed for $\bar{p}$. Although several technical challenges remain before final implementation, these results represent a significant step toward this new method of $\bar{H}$ production.

Acknowledgments

I would like to thank both of my supervisors, Eric Hunter and Chloé Malbrunot for their guidance and support throughout this summer. They were always willing to answer my many questions, and I learned a tremendous amount from them in such a short period of time. I would also like to thank the Institute of Particle Physics and TRIUMF for giving me the opportunity to participate in the CERN summer student programme. Lastly, thank you to the CERN summer student team and everyone I met along the way for an amazing summer.

References

[1] Luders, G. Proof of the TCP theorem. *Annals of Physics* **2**, 1–15 (2011). https://doi.org/10.1016/0003-4916(57)90032-5

[2] Sakharov, A.D. Violation of CP invariance, C asymmetry, and baryon asymmetry of the universe. *Sov. Phys. Usp.* **34**, 392 (1991). 10.1070/PU1991v034n05ABEH002497

[3] Hori, M., Sótér, A., Barna, D. et al. Two-photon laser spectroscopy of antiprotonic helium and the antiproton-to-electron mass ratio. *Nature* **475**, 484–488 (2011). https://doi.org/10.1038/nature10260

[4] Kuroda, N., Ulmer, S., Murtagh, D. et al. A source of antihydrogen for in-flight hyperfine spectroscopy. *Nat Commun* **5**, 3089 (2014). https://doi.org/10.1038/ncomms4089

[5] ASACUSA Collaboration. Status Report of ASACUSA AD-3 Collaboration for 2024. https://cds.cern.ch/record/2922834/files/SPSC-SR-358.pdf/

[6] Gabrielse, G., et al. Possible antihydrogen production using trapped plasmas. *Hyperfine Interactions* **44**, 287-293 (1989). https://doi.org/10.1007/BF02398677

[7] Ahmadi, M., et al. Antihydrogen accumulation for fundamental symmetry tests. *Nature* **8**, 681 (2017). https://doi.org/10.1038/s41467-017-00760-9

[8] Malmberg, J.H., Driscoll, C.F. Long-Time Containment of a Pure Electron Plasma. *Phys. Rev. Lett* **44**, 654 (1980). https://doi.org/10.1103/PhysRevLett.44.654

[9] Weiss, A. S. Simulating Antihydrogen Annihilation Distributions in ASACUSA's Cusp Trap. CERN (2022).

[10] Diermaier, M., Jepsen, C., Kolbinger, B. et al. In-beam measurement of the hydrogen hyperfine splitting and prospects for antihydrogen spectroscopy. *Nat Commun* **8**, 15749 (2017). https://doi.org/10.1038/ncomms15749

[11] Jonsell, Svante, and M. Charlton. Formation of antihydrogen beams from positron–antiproton interactions. *New J. Phys.* **21**, 073020 (2019). https://doi.org/10.1088/1367-2630/ab2bdc

[12] E. D. Hunter, A. Christensen, J. Fajans, T. Friesen, E. Kur, J. S. Wurtele. Electron cyclotron resonance (ECR) magnetometry with a plasma reservoir. *Phys. Plasmas* **27**, 032106 (2020). https://doi.org/10.1063/1.5141999

[13] Christensen, A. J. Exploiting Electron Magnetron Motion in a Penning-Malmberg Trap to Measure Patch Potentials, Misalignment, and Magnetic Fields. Doctoral Thesis, University of California, Berkeley (2024). https://escholarship.org/uc/item/9v9320jv

[14] Gorgadze, V., Pasquini, T., Fajans, J., Wurtele, J. Injection into electron plasma traps. *Lawrence Berkeley National Laboratory* (2003). https://escholarship.org/uc/item/3hg6f17r